ELSEVIER

Journal of Neuroscience Methods 54 (1994) 171–187

JOURNAL OF NEUROSCIENCE METHODS

Functional magnetic resonance imaging (FMRI) of the human brain

Edgar A. DeYoe [a,*], Peter Bandettini [b], Jay Neitz [a], David Miller [a], Paula Winans [a]

[a] *Department of Cellular Biology and Anatomy, Medical College of Wisconsin, 8701 Watertown Plank Road, Milwaukee, WI 53226, USA*
[b] *Department of Biophysics, Medical College of Wisconsin, 8701 Watertown Plank Road, Milwaukee, WI 53226, USA*

Received and accepted 28 June 1994

Abstract

Functional magnetic resonance imaging (FMRI) can provide detailed images of human brain that reflect localized changes in cerebral blood flow and oxygenation induced by sensory, motor, or cognitive tasks. This review presents methods for gradient-recalled echo-planar functional magnetic resonance imaging (FMRI). Also included is a discussion of the hypothesized basis of FMRI, imaging hardware, a unique visual stimulation apparatus, image post-processing and statistical analysis. Retinotopic mapping of striate and extrastriate visual cortex is discussed as an example application. The described echo-planar technique permitted acquisition of an image in 40 ms with a repetition rate of up to 2 per second. However, FMRI responses are slow compared to changes in neural activity. Onset of a visual checkerboard test pattern evoked a response that was delayed by 1–2 s and reached 90% of peak in 5 s. Return to baseline following stimulation was slightly slower. Alternating control (blank) and test (checkerboard) patterns every 20 s induced a cyclic response that was detected in the presence of noise using a cross-correlation technique that was verified by parametric statistics. FMRI revealed retinotopically organized patterns of visually evoked activity in response to annular stimuli that increased in visual field eccentricity. Retinotopy was also observed with test patterns rotated around the fixation point (center of gaze). Results from repeated tests 1 week apart were highly similar. Compared to passive viewing, an active visual discrimination task enhanced responses from extrastriate association cortex.

Keywords: Magnetic resonance imaging; Visual cortex; (Human)

1. Introduction

Brain images produced by functional magnetic resonance imaging (FMRI) reflect local changes in cerebral blood oxygenation evoked by sensory, motor or cognitive tasks (Bandettini et al., 1992b; Frahm et al., 1992; Kwong et al., 1992b; Ogawa et al., 1992; Turner et al., 1993c). Consequently, FMRI and other recently developed technologies have significantly expanded the possibilities for study of human cerebral function and pathology. In this respect, FMRI is potentially revolutionary since hundreds or even thousands of high-resolution images can be obtained from a single subject, thereby permitting detailed analysis of brain responses. Since it is non-invasive and has no significant health risks, FMRI will be applicable to a wide range of studies. Moreover, FMRI technology is one of the more accessible of the new scanning techniques since many hospitals and clinics include MRI facilities that could be modified to permit functional imaging.

To acquaint the non-specialist with this technology, we present here a review of the basic methodology, stressing those elements that we believe to be relatively unique to FMRI. Consequently, we do not review the fundamentals of conventional MRI and refer the interested reader to texts dealing specifically with that topic (Stark and Bradley, 1988; Schild, 1990). Since the field is evolving rapidly, we will not discuss all possible approaches to functional MRI, but will address many of the major technological issues.

1.1. Basis of the FMRI signal

MRI is based on the detection of electromagnetic signals (radio frequency (RF) waves) which emanate from spinning hydrogen protons when they are excited

* Corresponding author. Tel.: (414) 456-4920; E-mail: deyoe@its.mcw.edu.

SSDI 0165-0270(94)00095-6

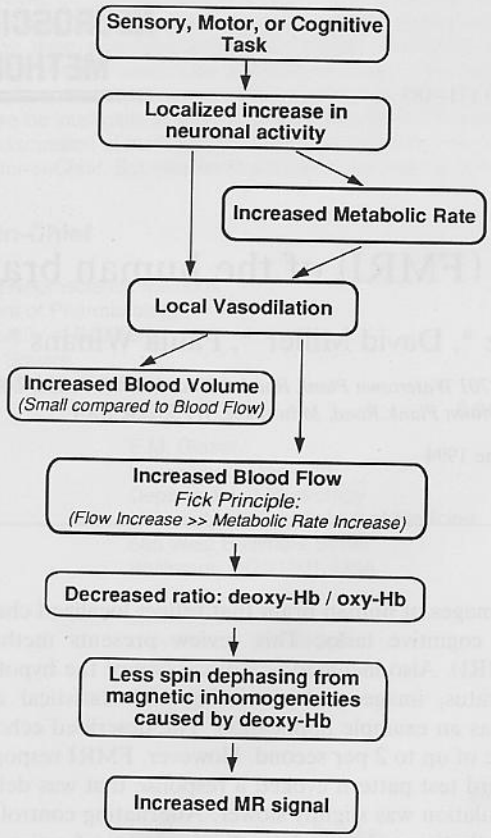

Fig. 1. Hypothesized mechanism of blood oxygenation level dependent (BOLD) contrast underlying common functional magnetic resonance imaging (FMRI) approaches. See text for discussion. Hb, hemoglobin.

by an RF pulse applied in the presence of an externally generated static magnetic field. Due to their abundance and ubiquitous distribution, hydrogen nuclei (single protons) provide the strongest MR signal in biological tissues. The RF pulse excites the spinning protons and causes their spins to become synchronized (phase locked) thereby allowing their individual contributions to add and produce a strong signal. Microscopic magnetic inhomogeneities (and other factors) within the tissue cause minute shifts in the RFs of nearby hydrogen protons within each voxel, ultimately causing them to fall out of synchronization (dephasing) which reduces the RF signal. Differences in the rate of dephasing (termed T2*) can indirectly reflect neuronal activity.

Fig. 1 summarizes the current understanding of the blood oxygenation level dependent (BOLD) mechanism whereby changes in neuronal activity affect the MR signal (Thulborn et al., 1982; Ogawa et al., 1990a,b, 1992, 1993; Ogawa and Tso-Ming, 1990; Turner et al., 1991, 1993c; Bandettini et al., 1992a,b, 1994a; Belliveau et al., 1992; DeCrespigny et al., 1992; Kwong et al., 1992b; Hoppel et al., 1993; Menon et al., 1993b; Jezzard et al., 1994; Kennan et al., 1994). A sensory, motor, or cognitive task produces a localized increase in neural activity. This results in a local vasodilatation that engenders a rapid increase in blood flow caused either by the production of metabolites or, more likely, due to a more direct effect on local blood vessels. The mechanism for this direct effect is poorly understood but may involve activity-dependent release of chemical factors such as nitric oxide, adenosine, hydrogen or potassium ions, or may involve a direct neuronal link to the vascular musculature (Lou et al., 1987; Iadecola, 1993). Whatever the cause, the change in blood flow and, consequently, oxygen delivery is 2–4 times greater than the corresponding increase in blood volume (Grubb et al., 1974). An excess of oxygenated hemoglobin is delivered to the activated region (Fox and Raichle, 1986; Fox et al., 1988) thereby reducing the amount of deoxy-hemoglobin within brain tissue voxels (Bandettini et al., 1992b; Kwong et al., 1992a). Deoxy-hemoglobin, but not oxy-hemoglobin, is paramagnetic (Pauling and Coryell, 1936; Thulborn et al., 1982; Weisskoff and Kiihne, 1992). Consequently, the presence of deoxy-hemoglobin in a capillary produces microscopic magnetic inhomogeneities that increase the dephasing of spinning hydrogen protons within a region extending approximately 2 times the radius of the vessel (Ogawa and Lee, 1992). As the quantity of deoxy-hemoglobin in the blood is washed out and diluted by the rising blood flow, less rapid dephasing occurs and the MR signal decays more slowly; these changes are picked up by the RF detector in the scanner. Ultimately, regions of the brain that have enhanced activity appear as brighter regions on the functional MR image. In addition, other activation-induced factors such as blood volume changes and proton movement effects can contribute to the MR signal changes. The magnitude of these effects can depend heavily on the particular imaging techniques used. (Henceforth, we will use the term 'FMR signal' to refer primarily to the deoxy-hemoglobin-based changes in the RF signal.)

In the following sections we describe our specific techniques for obtaining task-related FMRI images, for identifying foci with significant responses and for displaying the resulting functional images.

2. Materials and Methods

2.1. Scanner, pulse sequence

All images shown in this paper were obtained with a 1.5 T, General Electric Signa clinical scanner. The scanner was equipped with a custom 3-axis head coil designed for rapid gradient field switching. This permitted echo-planar imaging (EPI) in which a single

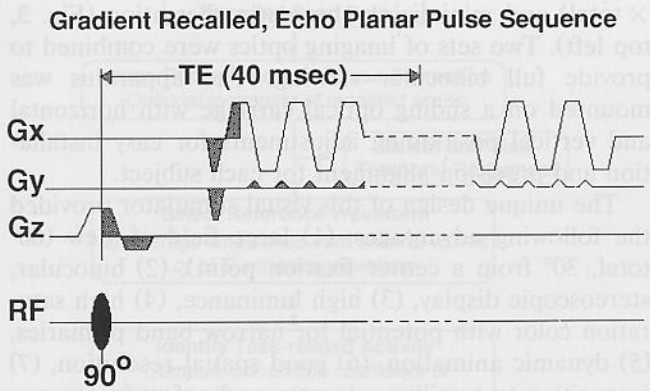

Fig. 2. Schematic of pulse sequence used to control gradient and RF fields for gradient-echo, echo-planar functional MRI. T_E, echo time; G_x, G_y, G_z, magnetic gradients along the x, y, and z axes of the scanner. G_z selects the slice of brain that will be activated by the RF pulse. G_x, G_y provide frequency and phase encoding of positions within the excited slice. RF, radio frequency excitation pulse that induces a spin flip of 90°.

image could be acquired in 40 ms (Wong et al., 1992a). To obtain high-quality images with similar sensitivity throughout the brain, the head coil also contained a shielded, transmit/receive 'birdcage' RF coil (Wong et al., 1992b). (The head coil system is commercially available through Medical Advances, Milwaukee, WI.) Spatial resolution was set by a 64×64 voxel matrix covering a 24×24 cm field of view with a slice thickness of 8–10 mm. This gave an in-plane pixel size of 3.75×3.75 mm.

Functional images will reflect changes in blood oxygenation if the MR signal is made sensitive to differences in the rate of proton spin dephasing (strictly, T2*, the effective decay rate of transverse magnetization). This can be accomplished with a gradient-recalled EPI sequence using an initial 90° RF pulse, an effective echo time (T_E) of 40 ms and an image repetition rate of 2 s ($T_R = 2.0$ s). Fig. 2 outlines the time course of the applied magnetic fields in the x, y, and z directions. The magnetic gradient, G_z, along the z axis (parallel to the scanner bore axis) determined which slice of brain was activated by the RF pulse. The G_x field established a gradient that encoded location on the x axis by the frequency of the proton spins. The G_y field added short 'blips' that shifted the phase of the proton spins for successive locations along the y axis. Thus each location within a slice was represented by a unique resonant frequency and phase. The whole se-

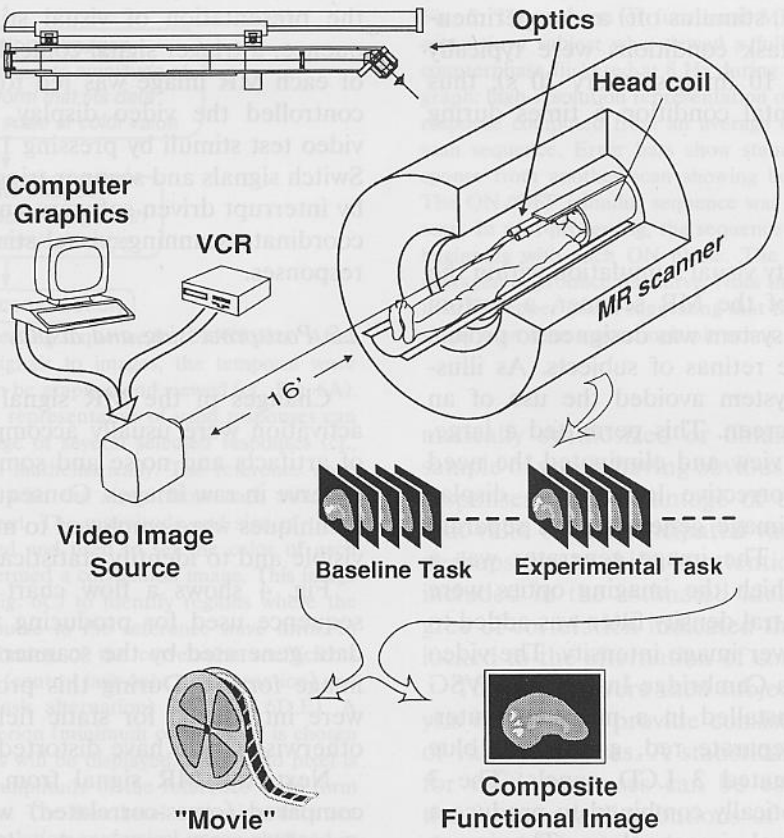

Fig. 3. Schematic of apparatus and experimental design for FMRI. The optical system for visual stimulation and the combined RF/gradient head coil are of custom design (Wong et al., 1992a,b). A typical experiment generates a temporal sequence of images. During the scan sequence, the subject is alternately engaged in a baseline (control) task and an experimental task (e.g., visual discrimination). Through post-processing, the sequence of images is displayed as a movie or a composite image that reflects changes in activation between baseline and experimental tasks.

quence was repeated for each image from each slice through the brain.

2.2. FMRI experiment design

A schematic of the basic organization of an FMRI experiment is shown in Fig. 3. For most experiments, 3 highly trained subjects were tested in multiple sessions using procedures reviewed by an internal advisory committee. Each subject was positioned supine inside the MR scanner with his head inside the head coil. The subject viewed a distant video image through a custom optical system. In a typical FMRI scan sequence, 110 successive echo-planar images were obtained at a rate of 1 every 2 s. The result was a temporal sequence of 100 brain images for each slice through the brain. The first 5–10 scans usually contained transients produced as the system settled to dynamic equilibrium. These images were discarded, except for the first, which provided a low-resolution anatomical image that was in register with the remaining functional images of the series. (The first image is proton density and T2* weighted due to an effectively infinite T_R. This highlights cerebrospinal fluid and makes the outline of the brain and sulci visible.) During multi-slice acquisition, 8–9 different slices were obtained during the same scan series. Control (e.g., stimulus off) and experimental (e.g., stimulus on) task conditions were typically alternated in blocks of 10 images (every 20 s), thus repeating the experimental condition 5 times during the scan sequence.

2.3. Sensory stimulation

To provide high-quality visual stimulation within the intense magnetic field of the MR scanner, a custom Maxwellian-view optical system was designed to project images directly onto the retinas of subjects. As illustrated in Fig. 3, this system avoided the use of an intervening projection screen. This permitted a large, high-luminance field of view and eliminated the need for subjects to wear corrective lenses. The display system consisted of an image generator and separate imaging optics (Fig. 3). The image generator was a video projector from which the imaging optics were removed. A variable neutral density filter was added to permit greater control over image intensity. The video projector was driven by a Cambridge Instruments VSG video graphics board installed in a micro-computer. Within the projector, separate red, green, and blue light beams transilluminated 3 LCD panels. The 3 separate panels were optically combined to produce a full color, 320×200 pixel, image plane. The image plane was viewed through a custom optical system that included a wide-field eyepiece, a 45° prism, and additional objective lenses for adjusting magnification (100 $\times$ total) and minimizing chromatic aberration (Fig. 3, top left). Two sets of imaging optics were combined to provide full binocular viewing. The apparatus was mounted on a sliding optical carriage with horizontal and vertical positioning adjustments for easy installation and precision alignment for each subject.

The unique design of this visual stimulator provided the following advantages: (1) large field of view (60° total, 30° from a center fixation point), (2) binocular, stereoscopic display, (3) high luminance, (4) high saturation color with potential for narrow band primaries, (5) dynamic animation, (6) good spatial resolution, (7) insensitive to pupillary changes and refractive errors, (8) non-magnetic, (9) independently positionable image generator and imaging optics, (10) physically compact (needs only 1.5″ clearance near eyes), and (11) versatile video format (computer-generated or video-taped images). The optical system has the disadvantage that large deviations of the eyes tend to block the view of the display. In addition, the setup and alignment of the system with naive subjects requires more time than some alternate methods.

2.4. Stimulus synchronization and response acquisition

To provide precise time synchronization between the presentation of visual stimuli and the scan sequence, a trigger signal coincident with the acquisition of each MR image was fed to a micro-computer that controlled the video display. Subjects responded to video test stimuli by pressing 1 of 2 response switches. Switch signals and scanner trigger pulses were detected by interrupt driven software and used to sequence and coordinate scanning, visual stimulation and behavioral responses.

2.5. Post-processing and display

Changes in the MR signal obtained during brain activation were usually accompanied by various types of artifacts and noise and sometimes were difficult to observe in raw images. Consequently, image processing techniques were employed to make the responses more visible and to identify statistically valid responses.

Fig. 4 shows a flow chart of the post-processing sequence used for producing functional images. Raw data generated by the scanner were first converted to image format. During this process, phase corrections were introduced for static field inhomogeneities that otherwise would have distorted the output image.

Next, the MR signal from each image voxel was compared (cross-correlated) with an ideal reference wave form representing the alternation of control and experimental tasks (Bandettini et al., 1993a). This helped to reduce artifacts and identify stimulus-locked responses. The reference wave form was either mathe-

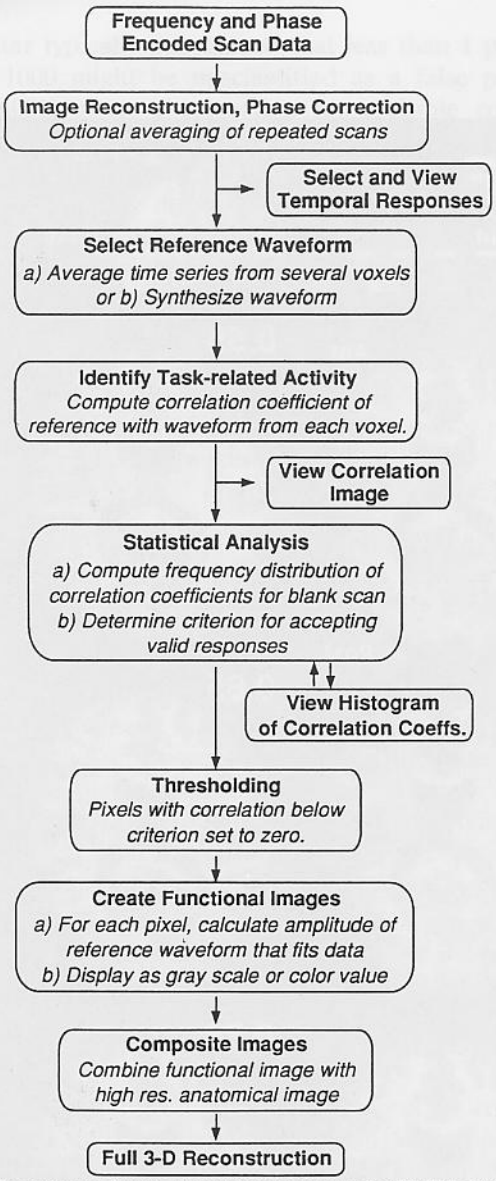

Fig. 4. Flow chart of post-processing sequence for FMRI data. After converting the raw scanner signals to images, the temporal wave form from individual voxels can be graphed and viewed (cf., Fig. 6A). A reference wave form that is representative of valid responses can be constructed from an average of several selected responses (cf., Fig. 6B) or can be synthesized mathematically. The reference wave form is then cross-correlated with the signal from each voxel to produce a correlation coefficient. The magnitude and sign of these coefficients can be color coded and used to set the color of each pixel in a new type of image termed a correlation image. This image can be viewed directly (cf., Fig. 6C) to identify regions where the response is similar in time course to the reference wave form. In addition, the frequency distribution of the correlation coefficients can be viewed for a blank scan (control task only, no alternation) and for the experimental scan (task alternation) (cf., Fig. 6D,E). A statistically valid response criterion (minimum correlation) is chosen and used to select which pixels will be displayed. Each valid pixel is color coded to represent the amplitude of the reference wave form that best fits the original data. The functional activation data are then combined with a high-resolution anatomical image obtained in the same session to yield the final functional image (cf., Fig. 6G). Both functional and anatomical data can be displayed as a full 3-dimensional reconstruction using software such as VoxelView (Vital Images).

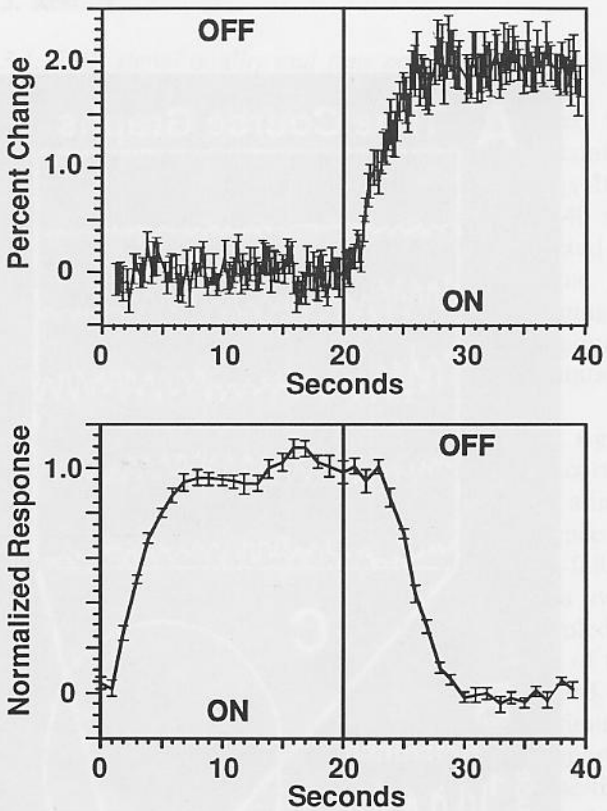

Fig. 5. Time course of functional MR signal from primary visual cortex in a subject who viewed a full-field checkerboard that was counterphase flickered at 8 Hz during the times marked ON. Upper graph: high-resolution representation of the rising phase of the FMR response computed from an average of 12 repetitions of the same scan sequence. Error bars show standard error. Lower graph: response from another scan showing both rising and falling phases. The ON/OFF stimulus sequence was repeated 12 times during the scan. In post-processing, the sequence was divided into 40 s epochs beginning with each ON phase. The successive epochs were then averaged to produce the curve. Note that standard errors are smaller than for upper graph suggesting that there is less variability within a single scan than across multiple scans.

matically synthesized or obtained empirically from a sample of voxels having obvious, robust, stimulus-locked responses. The advantage of the latter approach was that valid but unanticipated variations in the response, perhaps due to shifts in attention or alertness, could be included in the estimated ideal response. A high degree of correlation indicated that responses were time-locked to the alternation of control and test stimuli.

The images were then subjected to a statistical analysis in order to provide consistent, objective detection of valid responses. A statistically appropriate criterion for valid responses can be established by comparing the frequency distributions of cross-correlation coefficients obtained during an experimental scan series (task alternation) and during a blank control series having only the control stimulus (fixation point only, no task alternation). A threshold correlation of 0.55–0.65

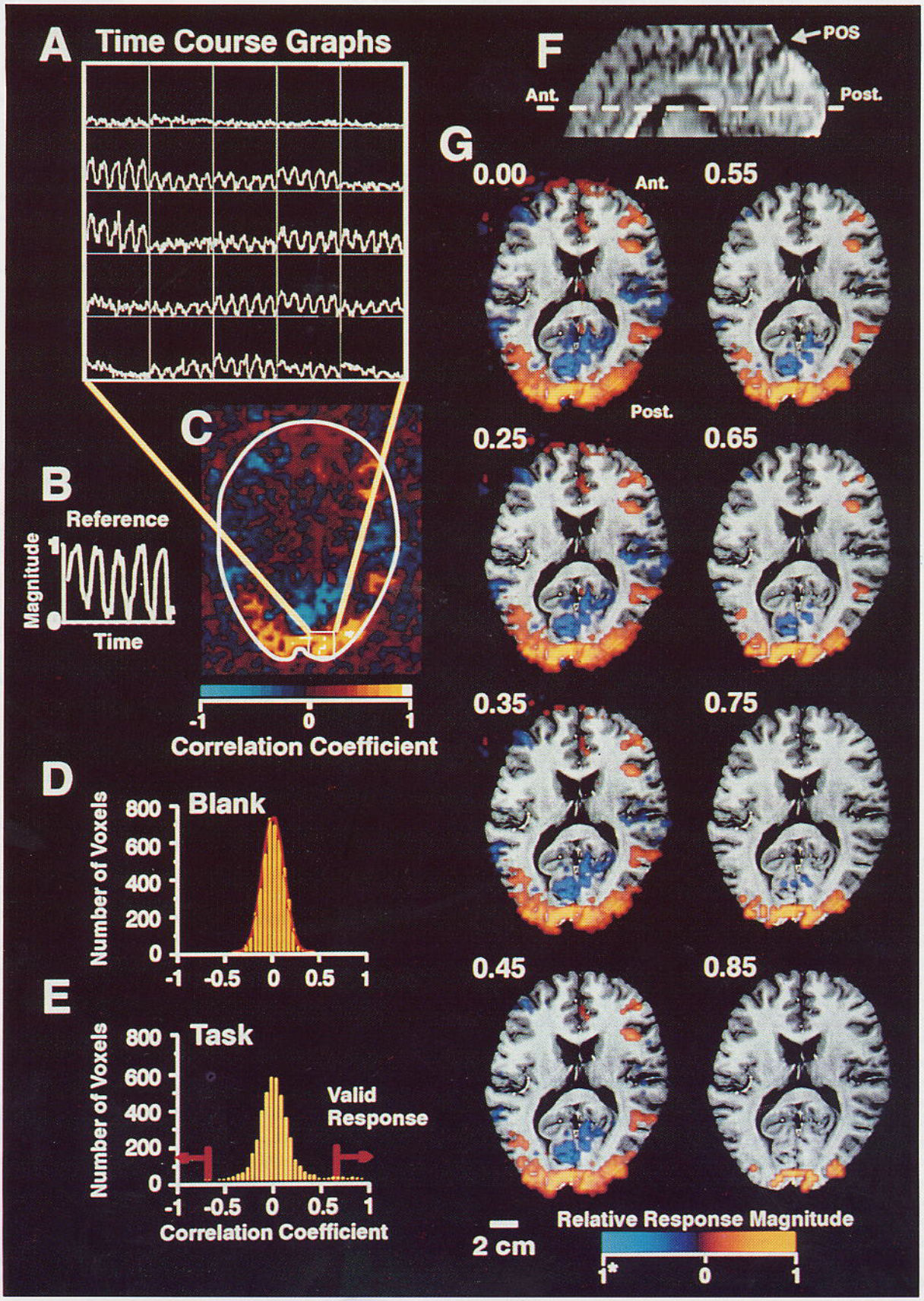
A
Time Course Graphs
B
Reference
Magnitude
1
Time
C
-1
0
1
Correlation Coefficient
D
Blank
Number of Voxels
800
600
400
200
0
-1
-0.5
0
0.5
1
E
Task
Valid
Response
Correlation Coefficient
F
POS
Ant.
Post.
G
0.00
Ant.
0.55
Post.
0.25
0.65
0.35
0.75
0.45
0.85
2 cm
Relative Response Magnitude
1*
0
1

or better typically guaranteed that less than 1 pixel in every 1000 might be misclassified as a false positive ($P < 0.001$, given a correction for multiple comparisons) (Hays, 1973).

Pixels having correlations less than the statistical criterion were not displayed in functional images. For pixels exceeding the criterion, a color scale was used to represent the amplitude of the reference wave form represented in the original empirical wave form (computed as the correlation coefficient multiplied by the variance of the original data: see Bandettini et al., 1993a). Thus, the final functional image showed the relative magnitudes of response for all pixels passing the statistical test for a stimulus-locked signal.

2.6. Registration of functional and anatomical images

Functional data were typically superimposed upon high-resolution anatomical MR images obtained with standard T1-weighted imaging techniques. However, FMR images can be susceptible to warping caused by large-scale magnetic field inhomogeneities (e.g., imperfect shimming or susceptibility anomalies due to air passages in the cranial bone). The first image in the FMRI series provided a low-resolution anatomical picture that was in exact registration with the subsequent functional images. Since this image was subject to the same warping effects, it could be compared with an undistorted high-resolution anatomical image obtained using a conventional pulse sequence. On rare occasions when distortions were present, they were corrected using an inverse warp technique (Jesmanowicz et al., 1992).

The final step in post-processing was to combine anatomical and functional data from all brain slices into a full volumetric reconstruction. This was accomplished with the aid of VoxelView software (Vital Images) which permitted independent manipulation of each data set and virtual slicing of the data in any desired imaging plane.

3. Results

3.1. FMR signal quality and time course

At strongly responding foci in visual cortex, the FMR signal typically changed 3–5% between control and test conditions although changes as high as 10% were occasionally recorded (1.5 T field, $T_E = 40$ ms, $T_R = 2.0$ s). Such responses were readily detected by examining the time course of the FMR signal for individual pixels (cf., Fig. 6A). However, averaging of multiple stimulus presentations significantly reduced signal variability, especially when the presentations were taken from a single scan series.

Fig. 5 illustrates the time course of the MR signal from a representative voxel in calcarine visual cortex. The bottom curve in Fig. 5 is the average of 12 stimulus repetitions obtained in a single scan sequence. It shows the time course of both the rising and falling phases of the response. Fig. 5 (top) shows data averaged from 12 separate scan series that were sampled at a higher rate in order to verify the time course of the rising phase. Note the somewhat higher standard errors. Both curves show that the delay from stimulus onset to the time at which the signal first departed from baseline was between 1 and 2 s and the rise-time to within 90% of peak was 5 s. In contrast, the delay from stimulus cessation to the beginning of a fall in signal intensity was longer, 3–4 s with a fall-time of nearly 7 s to within 10% of baseline. Thus there was some asymmetry in the rising and falling phases of the FMRI response. (Some investigators have described a short latency drop of $\sim 0.5\%$ in the FMR signal in the 1–2 s period between stimulus onset and the initial rise from baseline (K. Kwong, personal communication). As shown in Fig. 5 (top), this is not always evident.)

3.2. Image processing and valid response detection

Fig. 6 illustrates the use of the cross-correlation technique (Bandettini et al., 1993a) to detect valid

←

Fig. 6. Example of results of post-processing of responses in visual cortex to alternations of baseline and experimental tasks. A: multigraph display of the time course of the FMR signal from 25 voxels located near the occipital pole in primary visual cortex. The 200 s scan duration is represented by the width of each square in the multigraph display. Note cyclic responses to 5 alternations of a uniform blank field (stimulus off) with a counterphase flickered (8 Hz), checkered annulus of 6° diameter centered on a small fixation point. B: average reference wave form computed from 10 selected pixels. C: correlation image (axial view) showing the degree of correlation between the reference wave form and the response from each voxel in the slice. Color scale represents positive correlations in red/yellow, negative correlations by blues. D: distribution of correlation coefficients from a blank series (control task only, no alternation). Red curve shows gaussian function fitted to data. E: distribution of correlation coefficients taken from experimental scan represented by image C. Valid response criteria for both positive and negatively correlated responses shown by red arrows. F: sagittal view of brain showing plane of functional images. POS, parieto-occipital sulcus. G: composite functional images (axial view) for different correlation criteria shown by number next to each image. Color scale for functional data codes the magnitude of the reference wave form represented by the original data from each voxel (computed as the correlation coefficient multiplied by the variance of the original data (Bandettini et al., 1993a)). As correlation threshold increases, confidence in the validity of the displayed foci increases. For this case, a threshold of 0.65 yielded a probability of false-positive response of $P < 0.001$ (case CT).

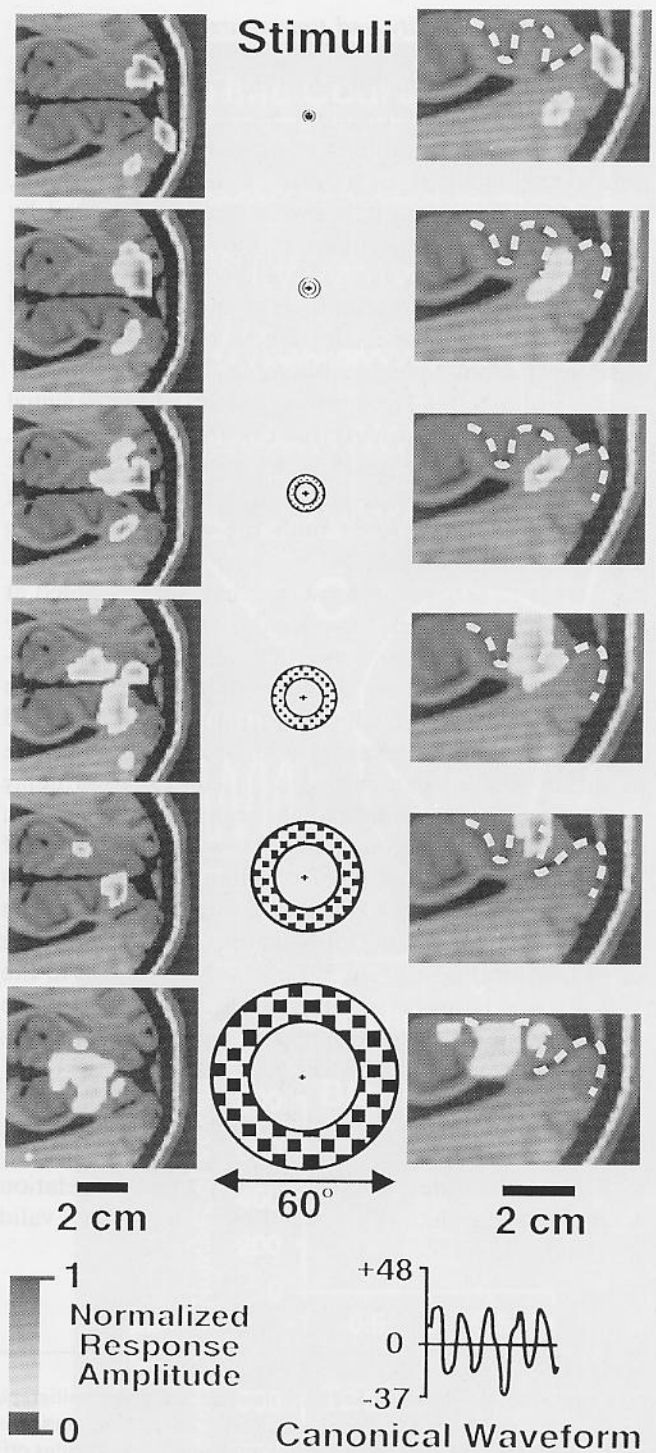

Fig. 7. Mapping visual field eccentricity in primary visual cortex of calcarine sulcus. Axial slice, occipital pole to right. Light-edged foci show sites where FMRI response correlated (> 0.55) with the canonical response wave form shown at bottom (X axis: time, full scale 200 s; Y axis: relative response magnitude). Shading within foci represents relative magnitude of response as indicated by the scale at bottom left. Checkered annuli were counterphase flickered at 8 Hz. FMR images in right column show details of enfolded cortex (dotted line) and activity in the lower hemisphere. (case AA) (Reprinted with permission of the author (DeYoe et al., 1994b)).

responses (DeYoe et al., 1994b). Fig. 6A shows a multi-graph display of the temporal FMR response for a group of 25 pixels located within the region of primary visual cortex outlined on the accompanying functional image. The responses were from a single scan and were not averaged. During the scan series, the subject viewed 5 repetitions of an 8 Hz counterphase flickering checkerboard annulus having a diameter of 6°. Time-locked responses were apparent for many pixels, although some clearly lacked stimulus-related responses (Fig. 6A). The reference wave form shown in Fig. 6B was computed as the average of responses from 10 selected pixels chosen from the responsive region. Fig. 6C illustrates the results of the cross-correlation between the reference wave form and the time course for each image pixel. Note that low correlation values were distributed ubiquitously throughout much of the image and background but that high correlation values were clustered in occipital cortex with some smaller foci in the right frontal lobe.

The frequency distribution of the correlation coefficients for the experimental task series and a blank control series are illustrated in Figs. 6E and 6D, respectively. The distribution for the blank series was closely approximated by a gaussian function (ignoring the $< 10^{-15}$ contribution of the 'tails' above 1.0 and below -1.0) and permitted estimation of the likelihood of mistakenly classifying a pixel as having a valid response (false positive) given a minimum correlation criterion. Fig. 6G illustrates functional images obtained for different correlation criteria. In these images, the data in pixels having correlations less than the criterion value (ignoring sign) were not displayed. In the remaining pixels, the amplitude of the reference wave form represented in the empirical data was coded using the color scale shown at the bottom of the figure.

For a correlation criterion of 0.65 the probability of obtaining false-positive responses was only about 1 pixel in 1000–10,000 given a conservative correction for multiple comparisons (Hays, 1973). At that criterion, artifacts due to subject motion and chance correlations were virtually eliminated. Close comparison between the resulting functional image (Fig. 6G, 0.65), the correlation image (Fig. 6C) and the multigraph displays (Fig. 6A) showed good correspondence between valid response foci and pixels having obvious stimulus-locked responses.

3.3. Example application: mapping visual field eccentricity

We previously reported (Miller et al., 1993; DeYoe et al., 1994a) that FMRI can be used to show the relationship between the position of a stimulus in the visual field and the location of activity in the visual cortex. Subjects passively viewed a counterphase modu-

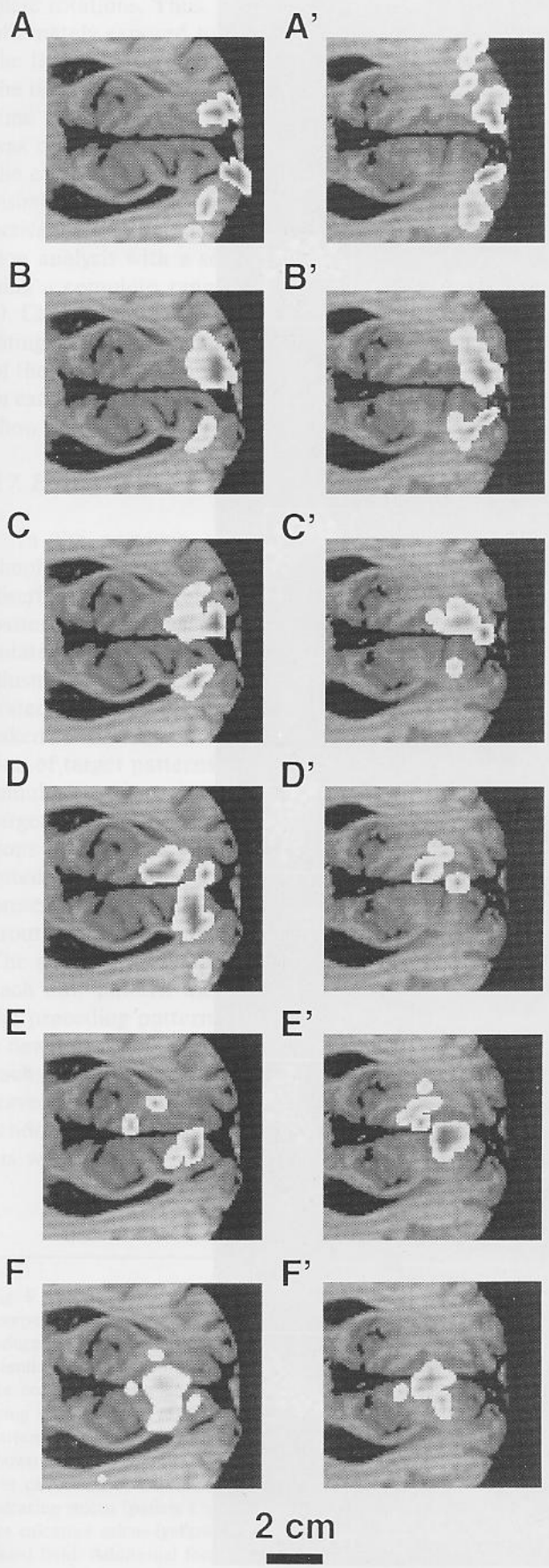

lated checkered annulus presented at a fixed eccentricity centered on a small fixation point. A different eccentricity was presented during each of 6 scan sequences. No averaging was used.

As illustrated in Fig. 7 (left column), a small (1.4°) checkered annulus elicited activation in striate cortex only at the occipital pole. Annuli presented at increasing eccentricities activated successively more anterior regions of the calcarine sulcus. The most eccentric annulus (24°) activated only the anterior calcarine while sparing the occipital pole.

The progression of activity foci was somewhat different in each hemisphere in part reflecting differences in the anatomy of the cortex or, perhaps, the fine pattern of vasculature innervation in each hemisphere. Detailed inspection of optimal sections (Fig. 7, right column) showed an orderly progression of foci that followed the circuitous course of the cortical mantle within the calcarine fissure of the right hemisphere (lower hemisphere in figure).

3.4. Repeatability

The results shown in Fig. 7 are shown again in Fig. 8 but are compared with data obtained from a repetition of the same experiment 1 week later. In this case, a mathematically synthesized reference wave form was used to perform identical cross-correlation analyses on both sets of data. The image slice planes were closely matched, although there was no deliberate attempt to make them identical. A good, although not perfect, correspondence between the 2 data sets is apparent. The most discrepant panels (A vs. A′ and D vs. D′) differ mainly in the appearance of a few additional foci that exceeded the correlation criterion for a valid response. These discrepancies might reflect variation in the location and orientation of the slice planes or, perhaps, variation in the subject's alertness (most experiments were run between 23:00 and 04:00 h!).

3.5. Mapping visual field angle by 'phase tagging'

Fig. 9 illustrates a method of mapping visual field topography that takes advantage of the phase of the cyclic FMR response. In this experiment, a checkered hemifield was rotated about the fixation point by 18° for each image (every 2 s) and continued for 5 com-

←

Fig. 8. Repeatability of FMRI activation patterns. A–F: same experiment as shown in Fig. 7 except reference wave form was a mathematically synthesized, full-wave rectified sine wave. A′–F′: data from the same experiment performed 1 week later. Same subject, stimulus and post-processing as A–F. Slice position is slightly different as evidenced by details of gyral patterns. Note similar patterns of activation in the 2 experiments (cases AA, AD).

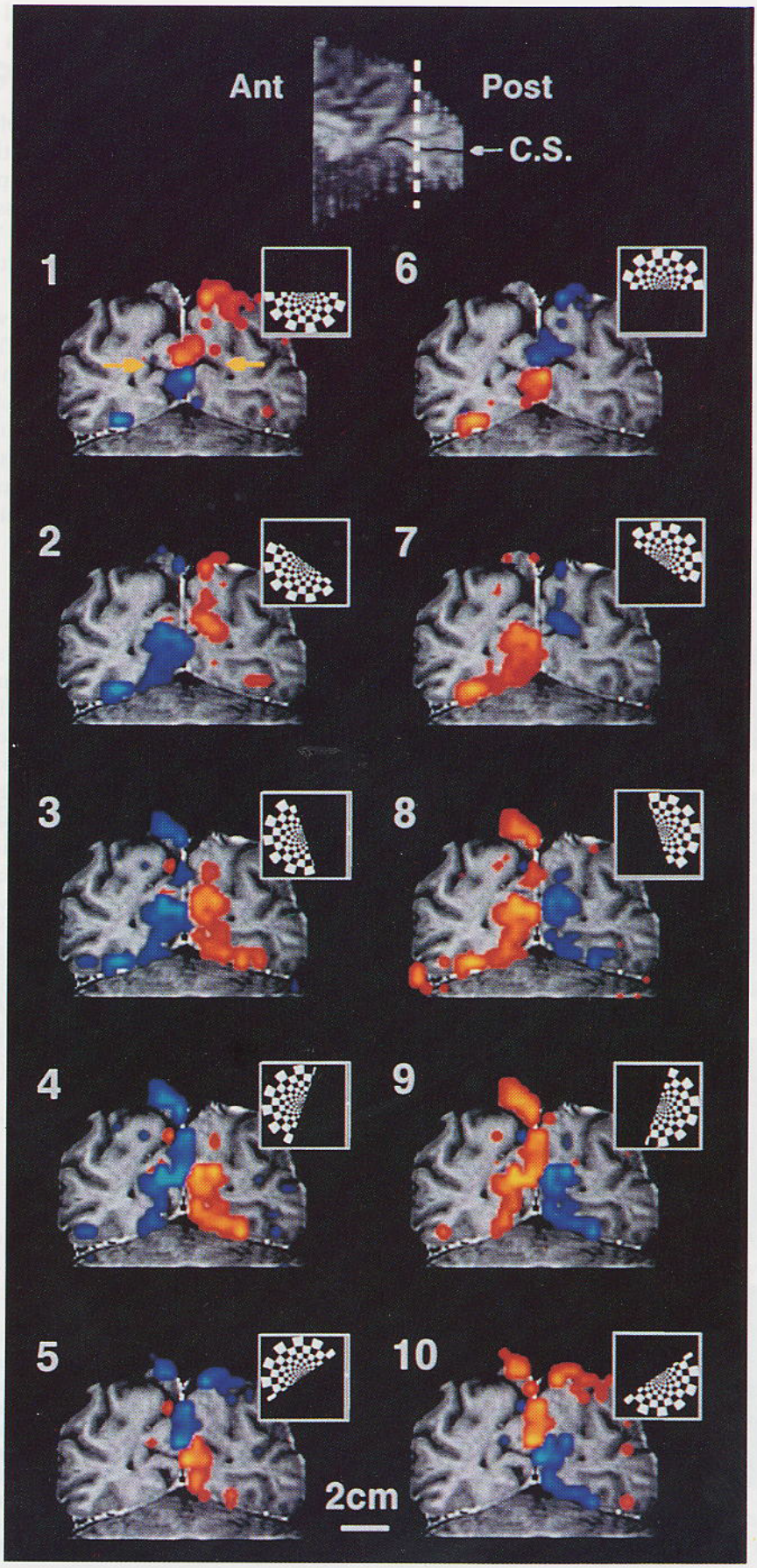
Ant
Post
C.S.
1
6
2
7
3
8
4
9
5
10
2cm

plete rotations. Thus, each point in the visual field was alternately exposed to the checkered hemifield 50% of the time and the blank hemifield 50% of the time but the timing varied with angular position. As a result, the time course at each responsive voxel in visual cortex was cyclic but had a phase (time delay) depending on the corresponding meridian (clock position) within the visual field. The complete progression of retinotopic activation was mapped by performing the cross-correlation analysis with a set of reference wave forms spanning a complete range of phase shifts (0–360° = 0–40 s). Close examination of the sequence reveals a circulating pattern encompassing the primary visual cortex of the calcarine sulcus. Additional regions of activation in extrastriate cortex dorsal and ventral to the calcarine show additional retinotopically organized regions.

3.7. Effects of active vs. passive task

In the previous experiment, the subject did not simply view the display passively but was asked to discriminate the relative eccentricity of a small test pattern superimposed on the checkered hemifield as it rotated. The advantage of using an active task was illustrated by results from another experiment illustrated in Fig. 10. In this experiment, subjects were asked to discriminate and report the spatial configuration of target patterns superimposed upon a checkered annulus used to map visual field eccentricity. The target patterns consisted of asymmetrical configurations of 3 groups of ellipsoid shapes that were delineated by a shifted checkerboard pattern. Successive presentations of the target pattern were either rotated around the center of the annulus or mirror-reversed. The subject's task was to press a button to indicate if each new pattern was rotated or mirrored relative to the preceding pattern. When the annulus was present, a new target pattern was shown immediately following each response (typically every 2–4 s). During the interleaved blank periods, subjects simply responded at random with roughly the same rate, although no stimulus was present on the screen. Fig. 10 illustrates the observed differences in the extent of activation of extrastriate cortex in the lingual and fusiform gyrii during both passive view and active discrimination tasks. Discrimination produced robust activation throughout a region that was only weakly active during passive viewing.

4. Discussion

FMRI holds exceptional promise as a tool for exploring human brain function since it is non-invasive, provides good spatial resolution, permits hundreds or even thousands of images to be obtained from a single subject, and is potentially available at hundreds of facilities operating clinical MRI scanners. Using the techniques described here, spatial localization of individual foci within a few millimeters can be achieved and differences of 1–2 s in the onset of activation can be differentiated. Imaging of association cortex as well as primary and secondary sensory and motor areas is readily obtained especially when using suitable behavioral tasks. With an RF coil designed to achieve uniform sensitivity, functional images encompassing virtually the entire cerebral cortex can be compared for a variety of task conditions.

Although FMRI has many advantageous features there are some potential limitations. It is not clear if all structures in the brain can be imaged equally well with FMRI. Areas near the base of the brain close to bone cavities and clusters of large blood vessels (e.g., Circle of Willis) may be particularly difficult to study due to magnetic field irregularities and blood pulsatility artifacts. However, there are preliminary reports that subcortical structures such as the lateral geniculate nucleus and spinal cord can be imaged (Frahm et al., 1993b; Yoshizawa et al., 1993). White matter and fiber tracts may not yield strong signals (Turner et al., 1991) presumably due to the relative paucity of vascularization and lower metabolic demand (Sokoloff et al., 1977; Duvernoy et al., 1981). Also, certain task manipulations may not induce activity changes that can be

←

Fig. 9. 'Phase tagging' of retinotopic activation in striate and extrastriate visual cortex. Top: sagittal view of occipital lobe showing plane of composite functional images displayed below. C.S., calcarine sulcus (also identified by yellow arrows in panel 1). 1–10: coronal views of activation induced by a flickering checkered hemifield that was rotated by 18° before each image acquisition (every 2 s). Five complete rotations of the stimulus were accomplished during the 200 s scan sequence. On each presentation, the subject was required to detect an increase or decrease in the eccentricity of a small black target randomly positioned within the checkered hemifield. Activation foci were detected by cross-correlation using a series of 20 reference wave forms that were delayed (phase shifted) by additive increments of 2 s. (Only 10 of the complete set of 20 patterns are shown here.) Foci shown in orange were optimally activated at a retinotopic position shown by the inset for each image. Activity foci shown in blue were maximally activated at a phase 180° later. The correspondence between stimulus phase (clock position) and evoked activation was calibrated by assuming that a stimulus centered on the vertical meridian evoked activity centered on the midline of the brain near the calcarine sulcus (panels 1 and 6). (This assumption is in accord with previous work in humans (Horton and Hoyt, 1991).) Note that activity near the calcarine sulcus (yellow arrows) circulates in a clockwise direction, sweeping through the complete angular representation of position in the visual field. Additional foci above and below the calcarine activation represent retinotopic organization in extrastriate visual areas (case DB).

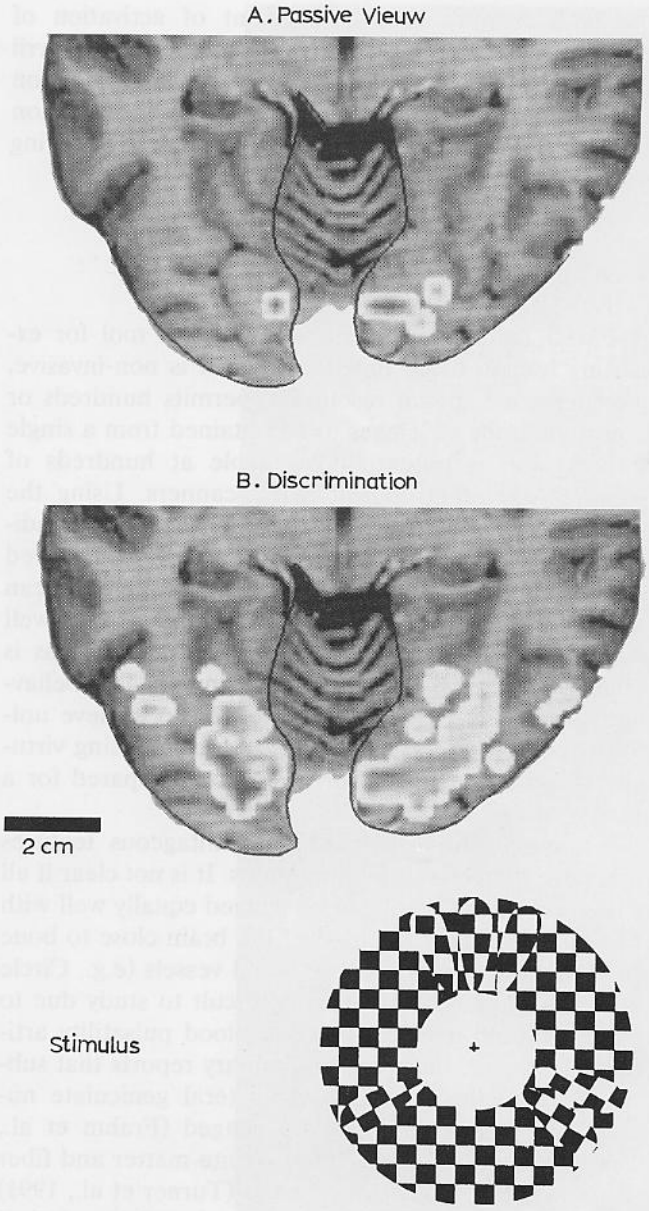

Fig. 10. Active discrimination task enhances activation of extrastriate cortex within ventral occipital cortex. (Note cerebellum visible between the hemispheres.) Stimulus and post-processing were identical for both task conditions but during active discrimination, subject indicated if global pattern of ellipsoid shapes superimposed on the annulus was rotated or mirror-imaged relative to immediately preceding stimulus.

resolved with FMRI. For example, neurons of visual cortex that code different directions of visual motion are intermingled on a microscopic scale (Born and Tootell, 1992). Consequently, a comparison of functional images obtained with rightward versus leftward motion might reveal little change. On the other hand, comparison of motion versus no motion, or motion vs. color, should be more successful since these tasks should differentially activate cells in cortical areas that are separated by relatively large distances (DeYoe and Van Essen, 1988; Corbetta et al., 1991b).

4.1. FMRI signal quality, noise and artifacts

With the techniques described here, the strongest activation-induced FMR signals had very good signal quality even without averaging. We have previously shown that the ratio of the mean signal change to the inherent variability of the FMR signal (Z score) for finger tapping responses in motor cortex ranged from 6.5 to 8.2 at a field strength of 1.5 T. Increasing static field strength improved the Z score to 10.5 (at 3.0 T) whereas lower field strengths yielded lower values (2.5 at 0.5 T) (Bandettini et al., 1994b). This indicates that simple sensory or motor tasks can induce a signal change that can be 7–10 standard deviations above the background 'noise' measured when the subject is at rest. However, the maximum signal change can vary significantly across the cortex depending on degree of activation, vascularization, voxel size, slice position, slice orientation and echo time. Very large signal changes of up to 30% have been reported when using small voxel sizes ($1 \times 1 \times 2$ mm), but these were often associated with large blood vessels (Lai et al., 1993). Moreover, it is evident that an important aspect of obtaining good FMR signals is the design of the behavioral task. This may be especially true for higher areas of 'association' cortex that can be strongly modulated by attentional factors (Corbetta et al., 1991a).

Although changes in blood oxygenation are thought to be the primary mechanism for FMRI, the recorded signals can also be affected by factors such as changes in blood volume, blood velocity, oxygen extraction fraction, pO_2, pCO_2, and hematocrit (Thulborn et al., 1982; Ogawa et al., 1990b, 1993; Kwong, 1992; Bandettini et al., 1994a; Jezzard et al., 1994). Movement of water protons relative to magnetic field inhomogeneities can also play a role (Hoppel et al., 1993; Kennan et al., 1994). Due to the complexity of these various factors, a comprehensive, quantitative model of the FMRI mechanism has yet to be developed. As a result, optimal imaging for a particular experimental goal requires careful consideration of the imaging protocol.

There are several sources of artifacts and noise that may contaminate FMRI images and complicate their interpretation. Large artifacts can arise from subject movements or pulse- and respiration-induced motion of the brain and vasculature (Hajnal et al., 1993). It is possible for such artifacts to be synchronized with stimulus presentation if the subject's position, arousal or other factors are not carefully matched between control and experimental conditions. Heart and respiration have also been shown to contribute periodic variations to the FMR signal that can appear as lower

(aliased) frequencies that add 'noise' to the recorded signals (Jezzard et al., 1992; Weisskoff et al., 1993; Biswal et al., 1994). Techniques such as cardiac or respiratory gating (synchronization) to minimize cyclic artifacts are difficult to apply in a straight forward manner since MR signal contrast is sensitive to small variations in the period between sequential acquisitions (T_R).

4.2. Spatial localization / resolution

The limits of FMRI spatial resolution have not yet been established definitively. At the time of this writing, there has not been a thorough study of the ability of FMRI to resolve two closely spaced, simultaneously active foci. The results reported here (Fig. 7) show that shifts of a few millimeters in the position of individual foci can be resolved when using a voxel size of 3.75×3.75 mm and a slice thickness of 4–8 mm. Smaller voxel sizes of $1.8 \times 1.8 \times 4$ mm have been used successfully for EPI (unpublished data) and voxels as small as $0.78 \times 0.78 \times 4.0$ mm have been used with slower multi-shot FMRI techniques (Frahm et al., 1993a). (In rats at 7 T, voxels as small as $0.117 \times 0.117 \times 0.5$ mm have been used with single-image acquisition times of 6–15 min (Ogawa et al., 1990b).) However, voxel size is not the only factor determining the effective resolution. The ability of FMR images to portray details of neuronal activation may be limited by biological rather than technological factors. Since FMRI depends on changes in oxygenation of blood within arterioles, capillaries and veinules, the vessel innervation density and the coupling of flow changes between adjacent vessel branches may limit the degree to which blood hemodynamics can reflect the fine pattern of neuronal activity. In addition, large veins and sinuses that drain distant regions of activation can sometimes generate signals that are displaced from the region of neuronal activity (Lai et al., 1993; Turner et al., 1993a). Although, recent experiments with high-resolution gradient-recalled imaging have suggested that many of the largest functional signals arise from blood vessels on the surface of the brain (Lai et al., 1993), this does not preclude contributions from small vessels and capillaries within the parenchyma. Recent experiments indicate that functional imaging with spin-echo rather than gradient-echo techniques may preferentially show signals from smaller vessels although with some sacrifice of overall signal amplitude (Bandettini et al., 1994a). The advantages of both approaches can be conserved by simultaneously acquiring both gradient-echo and spin-echo images. This has the added benefit that the size of blood vessels contributing to the signal in each voxel can be estimated (Bandettini et al., 1994a).

Despite the above concerns, the techniques described here demonstrate that FMRI can easily show detailed patterns of activity within individual cortical areas. Certainly the resolution available with current FMRI techniques is adequate for many experiments concerning the functional roles of macroscopic cortical areas.

4.3. Temporal resolution

The results reported here and elsewhere (DeYoe et al., 1992) show that local changes in deoxy-hemoglobin levels following cerebral activation are highly consistent but delayed and slowed relative to the underlying neuronal activity. More direct measures of cerebral function have a significantly faster time course. Single-cell responses in primary visual cortex typically begin within 40 ms of stimulus onset (Bartlett and Doty, 1974) and electrical potentials measured from the scalp have typical latencies of 10–100 ms (Martin, 1991). Although the sluggishness of the FMRI response is undoubtedly due to events subsequent to the neuronal activation, it is not yet clear if the limiting step is the triggering of local vasodilatation, the dynamics of blood flow, the clearing of deoxy-hemoglobin, or other factors. Nevertheless, the consistency of the MR signal permits resolution of time differences as small as 1–2 s. Thus, this technique may be capable of resolving some temporal features of complex cognitive or performance tasks involving extended cerebral activation, and it may be useful for observing the temporal sequence of activation associated with repetitive or multi-step behavioral tasks.

4.4. Post-processing techniques

Although good-quality FMRI signals can be easily observed in simple difference images, post-processing can greatly improve image quality and confidence in the interpretation of results. Although simple averaging and differencing techniques can be helpful, the use of the cross-correlation technique illustrated here and described by Bandettini et al. (1993a) makes use of the temporal properties of the signal to identify valid responses and to reduce or eliminate artifacts. A new type of image can be constructed by displaying correlation magnitudes for each pixel using different colors (Fig. 6C). This directly shows where task-related responses occur, but does not preserve information about response magnitude. A useful alternative is to display magnitude data in pixels that attain a correlation above a pre-selected minimum thereby showing differences in response amplitude for all valid pixels.

It is important to point out that the choice of reference wave form for the cross-correlation can affect details of the resulting images, although results tend to be similar for square, sine, rectified-sine and empirically derived reference functions (e.g., compare

Figs. 7 and 8). Empirically derived functions have the advantage that higher correlation values are typically obtained. In part, this is because legitimate variations in the response (e.g., variations in subject performance) are incorporated into the reference. On the other hand, mathematically synthesized wave forms avoid bias that could arise in the selection of data used to calculate empirical reference functions. However, choosing a synthesized reference is complicated by the lack of a completely satisfactory model that predicts the delay, smoothing and variability introduced by hemodynamic processes. In particular, variations in the delay (phase) of the response from voxel to voxel must be explicitly taken into account. Where such variations might be significant, several reference functions with different phase shifts can be used and the corresponding functional images compared. By presenting different stimulus conditions at different times during a scan sequence, it is possible to deliberately introduce delays in the responses of different activity foci. This 'phase tagging' can be used to map a wide range of stimulus values (e.g., retinotopic positions, Fig. 9) in a single scan sequence (also see Engel et al., 1993).

4.5. Statistical reliability

Besides enhancing signal-to-noise ratio and reducing artifacts, post-processing techniques can provide statistical tests of reliability for the resulting images. Simple statistical tests based on response magnitude (e.g., Z scores) may not reject artifacts having large, erratic peaks that can occur due to brain motion or pulsation. The cross-correlation approach used here greatly reduces these artifacts and provides a response measure that, for a blank trial (no task activation), is typically distributed as a gaussian function in the range from -1 to $+1$. (In theory there must be some discrepancy between the sampling distribution of a correlation coefficient and a gaussian, but practically the approximation is very close if the standard deviation is less than 0.2.) Consequently, deviations from this distribution due to task activation can be easily identified and the likelihood of mistakenly accepting a randomly high correlation as a valid response can be estimated.

4.6. Applications and significance of FMRI

Although still a new technology, FMRI has been used in a variety of studies, albeit many preliminary, that have begun to extend our understanding of cortical motor systems (Bandettini et al., 1993b; Berkelbach van der Sprenkel et al., 1993; Fieldman et al., 1993; Kim et al., 1993; Rao et al., 1993a,b), visual processing (DeYoe et al., 1993, 1994a; Engel et al., 1993; Schneider et al., 1993), auditory sound and language processing (Binder et al., 1993, 1994; Singh et al., 1993; Turner et al., 1993b), speech production (Benson et al., 1993; Cuenod et al., 1993a; Hinke et al., 1993; McCarthy et al., 1993; Rueckert et al., 1993), memory function (Blamire et al., 1993; Cohen et al., 1993) and cerebellar function (Bates et al., 1993; Cuenod et al., 1993b; Ellermann et al., 1993). A particularly intriguing application is the study of mental imagery (Le Bihan et al., 1992; Menon et al., 1993a; Rao et al., 1993a; Takahashi et al., 1993). The interpretation of such experiments requires a careful consideration of possible artifacts (e.g., shifts in attention) and different mental strategies that may be adopted by different subjects. Nevertheless, the ability to perform such experiments shows the tremendous potential of the FMRI technology.

A number of other studies have explored the use of FMRI for clinical applications such as pre-surgical identification of normal and diseased brain tissue (Cao et al., 1993; Connelly et al., 1993a; Jack et al., 1993), exploration of brain mechanisms underlying Alzheimer's disease (Mattay et al., 1993), obsessive compulsive disorders (Breiter et al., 1993), visual field defects (Sorensen et al., 1993), and epilepsy (Connelly et al., 1993b; Morris et al., 1994). Although such studies are primarily exploratory at the moment, the desire to apply this technology to clinical problems is strong.

FMRI will likely play an important role in defining and identifying functionally specialized areas of the cortex not only in vision but in virtually every other sensory, motor, and cognitive system. In conjunction with well-designed behavioral tasks, FMRI may also provide clues to the unique computations performed within different brain regions. Such insights could be invaluable for directing higher resolution studies using invasive techniques (e.g., optical imaging, single-unit recordings) to explore the cellular mechanisms of neuronal processing.

In summary, FMRI has the potential to become an extremely powerful tool not only in neuroscience but in a variety of clinical and academic fields. Hopefully, FMRI will facilitate studies in which previous knowledge about separate brain regions will be brought together to form a more integrated view of overall brain function. If even partially successful, FMRI will not only provide a significant advancement in our understanding of normal brain function but will also provide a powerful tool for the assessment and management of brain pathology.

Acknowledgements

We wish to thank Andre Jesmanowicz, Seth Glickman, Jay Kummer for development of analysis software, Dick Johnson for assistance in the design and construction of the optical system, Jon Wieser for technical assistance, and Eric Wong and James Hyde

for development of imaging coils and helpful discussions. This work was supported by NIH Grant EY10244 to E. DeYoe and Core Grant EY01931.

References

Bandettini, P.A., Wong, E.C., Hinks, R.S., Estkowski, L. and Hyde, J.S. (1992a) Quantification of changes in relaxation rates R2* and R2 in activated brain tissue. Proc. Soc. Magn. Reson. Med., 1: 719.

Bandettini, P.A., Wong, E.C., Hinks, R.S., Tikofsky, R.S. and Hyde, J.S. (1992b) Time course EPI of human brain function during task activation. Magn. Reson. Med., 25: 390–397.

Bandettini, P.A., Jesmanowicz, A., Wong, E.C. and Hyde, J.S. (1993a) Processing strategies for functional MRI of the human brain. Magn. Reson. Med., 30: 161–173.

Bandettini, P.A., Rao, S.M., Binder, J.R., Hammeke, J.R., Hammeke, T.A., Jesmanowicz, A., Yetkin, F.Z., Bates, S., Estkowski, L.D., Wong, E.C., Haughton, V.M., Hinks, R.S. and Hyde, J.S. (1993b) Magnetic resonance functional neuroimaging of the entire brain during performance and mental rehearsal of complex finger movement tasks. Proc. Soc. Magn. Reson. Med., 3: 1396.

Bandettini, P.A., Wong, E.C., Jesmanowicz, A., Hinks, R.S. and Hyde, J.S. (1994a) Spin-echo and gradient-echo EPI of human brain activation using BOLD contrast: a comparative study at 1.5 Tesla. Nucl. Magn. Reson. Biomed., in press.

Bandettini, P.A., Wong, E.C., Jesmanowicz, A., Prost, R., Cox, R.W., Hinks, R.S. and Hyde, J.S. (1994b) MRI of human brain activation at 0.5 T, 1.5 T, and 3.0 T: comparisons of R2* and functional contrast to noise ratio. Proc. Soc. Magn. Reson., 1: 434.

Bartlett, J.R. and Doty, R.W., Sr. (1974) Response of units in striate cortex of squirrel monkeys to visual and electrical stimuli. J. Neurophysiol., 4: 621–641.

Bates, S.R., Yetkin, F.Z., Bandettini, P.A., Jesmanowicz, A., Estkowski, L. and Haughton, V.M. (1993) Activation of the human cerebellum demonstrated by functional magnetic resonance imaging. Proc. Soc. Magn. Reson. Med., 3: 1420.

Belliveau, J.W., Kwong, K.K., Kennedy, D.N., Baker, J.R., Stern, C.E., Benson, R., Chesler, D.A., Weisskoff, R.M., Cohen, M.S., Tootell, R.B.H., Fox, P.T., Brady, T.J. and Rosen, B.R. (1992) Magnetic resonance imaging mapping of brain function. Human visual cortex. Invest. Radiol., 27: S59–S65.

Benson, R.R., Kwong, K.K., Belliveau, J.W., Baker, J., R., Cohen, M.S., Hildebrandt, N., Caplan, D.N. and Rosen, B.R. (1993) Selective activation of Broca's area and inferior parietal cortex for words using multislice gradient-echo EPI. Proc. Soc. Magn. Reson. Med., 3: 1398.

Berkelbach van der Sprenkel, J.W., Verheul, J., de Boer, R.W., van Yperen, G.H. and Luyten, P.R. (1993) Functional imaging of dominance in senso motor cortex of the human brain. Proc. Soc. Magn. Reson. Med., 3: 1424.

Binder, J.R., Rao, S.M., Hammeke, T.A., Bandettini, P.A., Jesmanowicz, A., Frost, J.A., Wong, E.C., Haughton, V.M. and Hyde, J.S. (1993) Temporal characteristics of functional magnetic resonance signal change in lateral frontal and auditory cortex. Proc. Soc. Magn. Reson. Med., 1: 5.

Binder, J.R., Rao, S.M., Hammeke, T.A., Yetkin, F.Z., Jesmanowicz, A., Bandettini, P.A., Wong, E.C., Estkowski, B.S., Goldstein, M.D., Haughton, V.M. and Hyde, J.S. (1994) Functional magnetic resonance imaging of human auditory cortex. Ann. Neurol., in press.

Biswal, B., DeYoe, E.A., Jesmanowicz, A. and Hyde, J.S. (1994) Removal of physiological fluctuations from functional MRI signals. Proc. Soc. Magn. Reson. Med., 2: 653.

Blamire, A.M., McCarthy, G., Nobre, A.C., Puce, A., Hyder, F., Bloch, G., Phelps, E., Rothman, D.L., Goldman-Rakic, P. and Shulman, R.G. (1993) Functional magnetic resonance imaging of human pre-frontal cortex during a spatial memory task. Proc. Soc. Magn. Reson. Med., 3: 1413.

Born, R.T. and Tootell, R.B. (1992) Segregation of global and local motion processing in primate middle temporal visual area. Nature, 357 (6378): 497–499.

Breiter, H.C., Kwong, K.K., Baker, J.R., Stern, C.E., Belliveau, J.W., Davis, T.L., Baer, L., O'Sullivan, R.M., Rauch, S.L., Savage, C.R., Cohen, M.S., Weisskoff, R.M., Brady, T.J., Jenike, M.A. and Rosen, B.R. (1993) Functional magnetic resonance imaging of symptom provocation in obsessive-compulsive disorder. Proc. Soc. Magn. Reson. Med., 1: 58.

Brindle, K.M., Brown, F.F., Campbell, I.D., Grathwohl, C. and Kuchel, P.W. (1979) Application of spin-echo nuclear magnetic resonance to whole-cell systems. Biochem. J., 180: 37–44.

Brooks, R.A. and Di Chiro, G. (1987) Magnetic resonance imaging of stationary blood: a review. Med. Phys., 14: 903–913.

Cao, Y., Towle, V.L., Levin, D.N., Grzeszczuk, R. and Mullan, J.F. (1993) Conventional 1.5 T functional MRI localization of human hand sensorimotor cortex with intraoperative electrophysiologic validation. Proc. Soc. Magn. Reson. Med., 3: 1417.

Cohen, J.D., Forman, S.D. and Casey, B.J. (1993) Spiral-scan imaging of dorsolateral prefrontal cortex during a working memory task. Proc. Soc. Magn. Reson. Med., 3: 1405.

Connelly, A., Gadian, D.G., Jackson, G.D., Kumar, V.J. and Harkness, W.F.J. (1993a) Presurgical identification of the motor cortex using functional MRI. Proc. Soc. Magn. Reson. Med., 3: 1422.

Connelly, A., Jackson, G.D., Cross, J.H. and Gadian, D.G. (1993b) Functional magnetic resonance imaging of focal seizures. Proc. Soc. Magn. Reson. Med., 1: 61.

Corbetta, M., Meizin, F.M., Shulman, G.L. and Petersen, S.E. (1991a) Selective attention modulates extrastriate visual regions in humans during visual feature discrimination and recognition. Ciba Foundation Symposium, 163: 165–180.

Corbetta, M., Miezin, F.M., Dobmeyer, S., Shulman, G.L. and Petersen, S.E. (1991b) Selective and divided attention during visual discrimination of shape, color, and speed: functional anatomy by positron emission tomography. J. Neurosci., 11: 2383–2402.

Cuenod, C.A., Bookheimer, S., Pannier, L., Posse, S., Bonnerot, V., Turner, R., Jezzard, P., Frank, J.A., Zeffiro, T. and Le Bihan, D. (1993a) Functional imaging during word generation using a conventional MRI scanner. Proc. Soc. Magn. Reson. Med., 3: 1414.

Cuenod, C.A., Zeffiro, T., Pannier, L., Posse, S., Bonnerot, V., Jezzard, P., Turner, R., Frank, J.A. and Le Bihan, D. (1993b) Functional imaging of the human cerebellum during finger movement with a conventional 1.5 T MRI scanner. Proc. Soc. Magn. Reson. Med., 3: 1421.

DeCrespigny, A.J., Wendland, M.F., Derugin, N., Kozniewska, E. and Moseley, M.E. (1992) Real-time observation of transient focal ischemia and hyperemia in cat brain. Magn. Reson. Med., 27: 391–397.

DeYoe, E.A. and Van Essen, D.C. (1988) Concurrent processing streams in monkey visual cortex. Trends Neurosci., 11: 219–226.

DeYoe, E.A., Neitz, J., Bandettini, P.A., Wong, E.C. and Hyde, J.S. (1992) Time course of event-related MR signal enhancement in visual and motor cortex. Proc. Soc. Magn. Reson. Med., 1: 1824.

DeYoe, E.A., Neitz, J., Miller, D. and Wieser, J. (1993) Functional magnetic resonance imaging (FMRI) of visual cortex in human subjects using a unique video graphics stimulator. Soc. Neurosci. Abst., 19: 424.

DeYoe, E.A., Neitz, J., Miller, D., Winans, P., Glickman, S. and Wieser, J. (1994a) Mapping multiple visual areas in human cerebral cortex. Invest. Ophthalmol. Vis. Sci., submitted.

Duvernoy, H.M., Delon, S. and Vannson, J.L. (1981) Cortical blood vessels of the human brain. Brain Res. Bull., 7: 519–579.

Ellermann, J.M., Flament, D., Kim, S.-G., Merkle, H., Fu, Q.-G., Ebner, T. and Ugurbil, K. (1993) Studies of human cerebellar function using multislice nuclear magnetic resonance imaging at high magnetic field. Proc. Soc. Magn. Reson. Med., 3: 1401.

Engel, S.A., Wandell, B.A., Rumelhart, D.E., Lee, A.T., Shadlen, M.N., Chichilinsky, E.J., Glover, G.H. and Newsome, W.T. (1993) Functional MRI measurements of human striate cortex topography. Soc. Neurosci. Abst., 19: 335.

Fieldman, J.B., Cohen, L.G., Jezzard, P., Pons, T., Sadato, N., Turner, R., LeBihan, D. and Hallett, M. (1993) Functional neuroimaging with echo-planar imaging in humans during execution and mental rehearsal of a simple motor task. Proc. Soc. Magn. Reson. Med., 3: 1416.

Fox, P.T. and Raichle, M.E. (1986) Focal physiological uncoupling of cerebral blood flow and oxidative metabolism during somatosensory stimulation in human subjects. Proc. Natl. Acad. Sci. USA, 83: 1140–1144.

Fox, P.T., Raichle, M.E., Mintun, M.A. and Dence, C. (1988) Nonoxidative glucose consumption during focal physiologic neural activity. Science, 241: 462–464.

Frahm, J., Bruhn, H., Merboldt, K. and Hanicke, W. (1992) Dynamic MRI of human brain oxygenation during rest and photic stimulation. J. Magn. Reson. Imaging, 2: 501–505.

Frahm, J., Merboldt, K.D. and Hanicke, W. (1993a) Functional MRI of human brain activation at high spatial resolution. Magn. Reson. Med., 29: 139–144.

Frahm, J., Merboldt, K.D., Hanicke, W., Kleinschmidt, A. and Steinmetz, H. (1993b) High-resolution functional MRI of focal subcortical activity in the human brain. Long-echo time FLASH of the lateral geniculate nucleus during visual stimulation. Proc. Soc. Magn. Reson. Med., 1: 57.

Grubb, R.L., Raichle, M.E., Eichling, J.O. and Ter-Pogossian, M.M. (1974) The effects of changes in $PaCO_2$ on cerebral blood volume, blood flow, and vascular mean transit time. Stroke, 5: 630–639.

Hajnal, J.V., Oatridge, A., Schwieso, J., Cowan, F.M., Young, I.R. and Bydder, G.M. (1993) Cautionary remarks on the role of veins in the variability of functional imaging experiments. Proc. Soc. Magn. Reson. Med., 1: 166.

Hays, W.L. (1973) Statistics for the Social Sciences, 1st edn., Holt, Rinehart and Winston, New York.

Hinke, R.M., Hu, X., Stillman, A.E., Kim, S.-G., Merkle, H., Salmi, R. and Ugurbil, K. (1993) Functional magnetic resonance imaging of Broca's area during internal speech. Neuroreport, 4: 675–678.

Hoppel, B.E., Weisskoff, R.M., Thulborn, K.R., Moore, J.B., Kwong, K.K. and Rosen, B.R. (1993) Measurements of regional blood oxygenation and cerebral hemodynamics. Magn. Reson. Med., 30: 715–723.

Horton, J.C. and Hoyt, W.F. (1991) The representation to the visual field in human striate cortex. a revision of the classic holmes map. Arch. Ophthalmol., 109: 816–824.

Iadecola, C. (1993) Regulation of the cerebral microcirculation during neural activity: is nitric oxide the missing link? Trends Neurosci., 16: 206–214.

Jack, C.R., Thompson, R., Sharbrough, F.W., Kelly, P.J., Butts, R.K., Hangiandreou, N.J., Riederer, S.J., Ehman, R.L. and Cascino, G.D. (1993) Presurgical mapping of the sensory motor cortex with functional MRI. Proc. Soc. Magn. Reson. Med., 3: 1423.

Jesmanowicz, A., Wong, E.C., DeYoe, E.A. and Hyde, J.S. (1992) Method to correct anatomic distortion in echo planar images. Proc. Soc. Magn. Reson. Med., 2: 4260.

Jezzard, P., Heineman, F., Taylor, J., Depres, D., Wen, H. and Turner, R. (1992) Comparison of EPI gradient-echo contrast changes in cat brain caused by respiratory challenges with direct simultaneous spectrophotometric evaluation of cerebral oxygenation via a cranial window. Proc. Soc. Magn. Reson. Med., 918.

Jezzard, P., Heineman, F., Taylor, J., DesPres, D., Wen, H., Balaban, R.S. and Turner, R. (1994) Comparison of EPI gradient-echo contrast changes in cat brain caused by respiratory challenges with direct simultaneous evaluation of cerebral oxygenation via a cranial window. Nucl. Magn. Reson. Biomed., in press.

Kennan, R.P., Zhong, J. and Gore, J.C. (1994) Intravascular susceptibility contrast mechanisms in tissues. Magn. Reson. Med., 31: 9–21.

Kim, S.-G., Ashe, J., Hendrich, K., Ellerman, J.M., Merkle, H., Ugurbil, K. and Georgopoulos, A.P. (1993) Functional magnetic resonance imaging of motor cortex: hemispheric asymmetry and handedness. Science, 261: 615–617.

Kwong, K.K., Belliveau, J., W., Stern, C.E., Chesler, D.A., Goldberg, I.E., Poncelet, B.P., Kennedy, D.N., Weisskoff, R.M., Cohen, M.S., Turner, R., Cheng, H.M., Brady, T.J. and Rosen, B.R. (1992a) Functional MR imaging of primary visual and motor cortex. J. Magn. Reson. Imaging, 2: 76.

Kwong, K.K., Belliveau, J.W., Chesler, D.A., Goldberg, I.E., Weisskoff, R.M., Poncelet, B.P., Kennedy, D.N., Hoppel, B.E., Cohen, M.S., R., T., Cheng, H., Brady, T.J. and Rosen, B.R. (1992b) Dynamic magnetic resonance imaging of human brain activity during primary sensory stimulation. Proc. Natl. Acad. Sci. USA, 89: 5675–5679.

Lai, S., Hopkins, A.L., Haacke, E.M., Li, D., Wasserman, B.A., Buckley, P., Friedman, L., Meltzer, H., Hedera, P. and Friedland, R. (1993) Identification of vascular structures as a major source of signal contrast in high resolution 2D and 3D functional activation imaging of the motor cortex at 1.5T: preliminary results. Magn. Reson. Med., 30: 387–392.

Le Bihan, D., Turner, R., Jezzard, P., Cuenod, J.A. and Zeffiro, T. (1992) Activation of human visual cortex by mental representation of visual patterns. Proc. Soc. Magn. Reson. Med., 1: 311.

Lou, H.C., Edvinsson, L. and MacKenzie, E.T. (1987) The concept of coupling blood flow to brain function: revision required?, Ann. Neurol., 22: 289–297.

Martin, J.H. (1991) The collective electrical behavior of cortical neurons: the electroencephalogram and the mechanisms of epilepsy. In: E.R. Kandel, J.H. Schwartz and T.M. Jessel (Eds.), Principles of Neural Science, Elsevier, New York, pp. 777–791.

Mattay, V.S., Frank, J.A., Sunderland, T., Barrios, F., Sobering, G., Moonen, C.T.W., Sexton, R.S. and Weinberger, D.R. (1993) Dynamic contrast functional MRI of Alzheimer's disease during visual activation. Proc. Soc. Magn. Reson. Med., 3: 1404.

McCarthy, G., Blamire, A.M., Bloch, G., Rothman, D.L. and Shulman, R.G. (1993) Echo planar MRI studies of frontal cortex during word generation. Proc. Soc. Magn. Reson. Med., 3: 1412.

Menon, R., Ogawa, S., Tank, D.W., Ellermann, J.M., Merkle, H. and Ugurbil, K. (1993a) Visual mental imagery by functional brain MRI. Proc. Soc. Magn. Reson. Med., 3: 1381.

Menon, R.S., Ogawa, S., Tank, D. and Ugurbil, K. (1993b) 4 Tesla gradient recalled echo characteristics of photic stimulation-induced signal changes in the human primary visual cortex. Magn. Reson. Med., 30: 380–386.

Miller, D.L., DeYoe, E.A., Neitz, J., Bandettini, P.A. and Hyde, J.S. (1993) Mapping of the human visual cortex utilizing functional magnetic resonance imaging (FMRI) Invest. Ophthalmol. Vis. Sci., Suppl. 34: 813.

Morris, G.L., Mueller, W.M., Yetkin, F.Z., Haughton, V.M., Hammeke, T.A., Swanson, S., DeYoe, E.A., Rao, S.M., Binder, J.R., Estkowski, L.D., Bandettini, P.A., Wong, E.C. and Hyde, J.S. (1994) Functional magnetic resonance imaging in partial epilepsy. Epilepsia, in press.

Ogawa, S. and Lee, T.M. (1992) Blood oxygenation level dependent MRI of the brain: Effects of seizure induced by kainic acid in rat. Proc. Soc. Magn. Reson. Med., 1: 501.

Ogawa, S. and Tso-Ming, L. (1990) Magnetic resonance imaging of blood vessels at high fields: in vivo and in vitro measurements and image simulation. Magn. Reson. Med., 16: 9–18.

Ogawa, S., Lee, T., Nayak, S. and Glynn, P. (1990a) Oxygenation-sensitive contrast in magnetic resonance image of rodent brain in high magnetic fields. Magn. Reson. Med., 14: 68–78.

Ogawa, S., Lee, T.M., Kay, A.R. and Tank, D.W. (1990b) Brain magnetic resonance imaging with contrast dependent on blood oxygenation. Proc. Natl. Acad. Sci. USA, 87: 9868–9872.

Ogawa, S., Tank, D.W., Menon, R., Ellermann, J.M., Kim, S., Merkle, H. and Ugurbil, K. (1992) Intrinsic signal changes accompanying sensory stimulation: Functional brain mapping using MRI. Proc. Natl. Acad. Sci., 89: 5951–5955.

Ogawa, S., Menon, R.S., Tank, D.W., Kim, S.-G., Merkle, H., Ellerman, J.M. and Ugurbil, K. (1993) Functional brain mapping by blood oxygenation level-dependent contrast magnetic resonance imaging. Biophys. J., 64: 803–812.

Pauling, L. and Coryell, C.D. (1936) The magnetic properties and structure of hemoglobin, oxyhemoglobin, and corbonmonoxyhemoglobin. Proc. Natl. Acad. Sci. USA, 22: 210–216.

Rao, S.M., Binder, J.R., Bandettini, P.A., Hammeke, T.A., Yetkin, F.Z., Jasmanowicz, A., Lisk, L.M., Morris, G.L., Mueller, W.M., Estkowski, L.D., Wong, E.C., Haughton, V.M. and Hyde, J.S. (1993a) Functional magnetic resonance imaging of complex human movements. Neurology, 43: 2311–2318.

Rao, S.M., Binder, J.R., Hammeke, T.A., Lisk, L.M., Bandettini, P.A., Yetkin, F.Z., Morris, G.L., Mueller, W.M., Antuono, P.G., Wong, E.C., Haughton, V.M. and Hyde, J.S. (1993b) Somatotopic mapping of the primary motor cortex with functional magnetic resonance imaging. Soc. Magn. Reson. Imaging Med. Abst., 3: 1397.

Rueckert, L., Appollonia, I., Gratman, J., Jezzard, P., Johnson Jr., R., Le Bihan, D. and Turner, R. (1993) Functional activation of left frontal cortex during covert word production. Proc. Soc. Magn. Reson. Med., 1: 60.

Schild, H. (1990) MRI Made Easy (... well almost). H. Heeneman, Berlin.

Schneider, W., Noll, D.C. and Cohen, J.D. (1993) Functional topographic mapping of the cortical ribbon in human vision with conventional MRI scanners. Nature, 365: 150–153.

Singh, M., Kim, H., Kim, T., Khosla, D. and Colletti, P. (1993) Functional MRI at 1.5T during auditory stimulation. Proc. Soc. Magn. Reson. Med., 3: 1431.

Sokoloff, L., Reivich, M., Kennedy, C., Des Rosiers, M.H., Patlak, C.S., Pettigrew, K.D., Sakurada, O. and Shinohara, M. (1977) The [14C]deoxyglucose method for the measurement of local cerebral glucose utilization: theory, procedure, and normal values in the conscious and anesthetized albino rat. J. Neurochem., 28: 897–916.

Sorensen, A.G., Caramis, F., Wray, S.H., Kwong, K., Belliveau, J., Stern, C., Baker, J., Gazit, I., Breiter, H. and Rosen, B. (1993) Extrastriate activation in patients with visual defects. Proc. Soc. Magn. Reson. Med., 1: 62.

Stark, D.D. and Bradley, W.G. (Ed.) (1988) Magnetic Resonance Imaging. C.V. Mosby, St. Louis.

Takahashi, T., Takiguchi, K., Itagaki, H., Onodera, Y., Yamamoto, E. and Koizumi, H. (1993) Real time imaging of brain activation during imagination of finger tasks. Proc. Soc. Magn. Reson. Med., 3: 1415.

Thulborn, K.R., Waterton, J.C., Matthews, P.M. and Radda, G.K. (1982) Oxygenation dependence of the transverse relaxation time of water protons in whole blood at high field. Biochim. Biophys. Acta, 714: 265–270.

Turner, R., Le Bihan, D., Moonen, C.T.W., Despres, D. and Frank, J. (1991) Echo-Planar time course MRI of cat brain oxygenation changes. Magn. Reson. Med., 22: 159–166.

Turner, R., Jezzard, P., Le Bihan, D. and Prinster, A. (1993a) Contrast mechanisms and vessel size effects in BOLD contrast functional neuroimaging. Proc. Soc. Magn. Reson. Med., 1: 173.

Turner, R., Jezzard, P., Le Bihan, D., Prinster, A., Pannier, L. and Zeffiro, T. (1993b) BOLD contrast imaging of cortical regions used in processing auditory stimuli. Proc. Soc. Magn. Reson. Med., 3: 1411.

Turner, R., Jezzard, P., Wen, H., Kwong, K.K., LeBihan, D., Zeffiro, T. and Balaban, R.S. (1993c) Functional mapping of the human visual cortex at 4 and 1.5 Tesla using deoxygenation contrast EPI. Magn. Reson. Med., 29: 277–279.

Weisskoff, R.M. and Kiihne, S. (1992) MRI Susceptometry: Image-based measurement of absolute susceptibility of MR contrast agents and human blood. Magn. Reson. Med., 24: 375–383.

Weisskoff, R.M., Baker, J., Belliveau, J., Davis, T.L., Kwong, K.K., Cohen, M.S. and Rosen, B.R. (1993) Power spectrum analysis of functionally-weighted MR data: what's in the noise?. Proc. Soc. Magn. Reson. Med., 1: 7.

Wong, E.C., Bandettini, P.A. and Hyde, J.S. (1992a) Echo-planar imaging of the human brain using a three axis local gradient coil. Proc. Soc. Magn. Reson. Med., 1: 105.

Wong, E.C., Boskamp, E. and Hyde, J.S. (1992b) A volume optimized quadrature elliptical endcap birdcage brain coil. Proc. Soc. Magn. Reson. Med., 2: 4015.

Yoshizawa, T., Sanders, J.A., Moore, G.J., McKay, M.D., Nose, T. and Sillerud, L.O. (1993) Functional MRI of spinal cord activity during a motor task. Proc. Soc. Magn. Reson. Med., 1: 55.